Archival Report

Altered Intrinsic Functional Brain Architecture in Children at Familial Risk of Major Depression

Xiaoqian J. Chai, Dina Hirshfeld-Becker, Joseph Biederman, Mai Uchida, Oliver Doehrmann, Julia A. Leonard, John Salvatore, Tara Kenworthy, Ariel Brown, Elana Kagan, Carlo de los Angeles, John D.E. Gabrieli, and Susan Whitfield-Gabrieli

ABSTRACT

BACKGROUND: Neuroimaging studies of patients with major depression have revealed abnormal intrinsic functional connectivity measured during the resting state in multiple distributed networks. However, it is unclear whether these findings reflect the state of major depression or reflect trait neurobiological underpinnings of risk for major depression.

METHODS: We compared resting-state functional connectivity, measured with functional magnetic resonance imaging, between unaffected children of parents who had documented histories of major depression (at-risk, $n = 27$; 8–14 years of age) and age-matched children of parents with no lifetime history of depression (control subjects, $n = 16$).

RESULTS: At-risk children exhibited hyperconnectivity between the default mode network and subgenual anterior cingulate cortex/orbital frontal cortex, and the magnitude of connectivity positively correlated with individual symptom scores. At-risk children also exhibited 1) hypoconnectivity within the cognitive control network, which also lacked the typical anticorrelation with the default mode network; 2) hypoconnectivity between left dorsolateral prefrontal cortex and subgenual anterior cingulate cortex; and 3) hyperconnectivity between the right amygdala and right inferior frontal gyrus, a key region for top-down modulation of emotion. Classification between at-risk children and control subjects based on resting-state connectivity yielded high accuracy with high sensitivity and specificity that was superior to clinical rating scales.

CONCLUSIONS: Children at familial risk for depression exhibited atypical functional connectivity in the default mode, cognitive control, and affective networks. Such task-independent functional brain measures of risk for depression in children could be used to promote early intervention to reduce the likelihood of developing depression.

Keywords: Chidren, Default mode network, Depression, Familial risk, Resting-state fMRI, Subgenual ACC

http://dx.doi.org/10.1016/j.biopsych.2015.12.003

Neuroimaging in patients with major depression (major depressive disorder [MDD]) has revealed abnormal activation patterns in multiple brain networks, including the default mode network (DMN) and cognitive control and affective networks. The DMN, anchored in the medial prefrontal cortex (mPFC) and posterior cingulate cortex (PCC), is suppressed in healthy adults during tasks that demand external attention but does not show the typical pattern of task-induced deactivation in adults and adolescents with MDD (1–3). The cognitive control network, including the dorsolateral prefrontal cortex (DLPFC), which is typically activated during cognitively demanding tasks, has shown decreased activation in adults with MDD (4,5). The affective network includes the amygdala and other limbic region structures (6,7) and, most saliently for MDD, the subgenual anterior cingulate cortex (sgACC), which is considered a core region in the functional and structural pathophysiology of MDD (8–10). The affective network exhibits abnormal activation patterns during emotion processing in adults with MDD (11–13). These abnormal activations in distributed networks may account for corticolimbic dysregulation in MDD (8,14).

Mirroring these brain activation abnormalities, patients of different ages with MDD have shown abnormal intrinsic functional connectivity of the brain measured via resting-state functional magnetic resonance imaging (rs-fMRI) (15). First, increased resting-state connectivity within the DMN and between the DMN and sgACC has been reported in adults (16,17) and adolescents (18) with MDD. Hyperconnectivity of sgACC correlated with duration of current depressive episodes in adults (16) and with emotional dysregulation in pediatric depression (19). These results support the possibility that DMN-sgACC hyperconnectivity might underlie depressive rumination (20). Second, several studies reported decreased resting-state connectivity within the cognitive control network in adult patients with MDD (21–23). In line with this evidence, MDD has been conceptualized as an imbalance between the DMN and the cognitive control network (24–26). Third, atypical connectivity between the amygdala and cortical structures has

been found in adults (27,28) and children (29) with MDD and is thought to reflect deficits in emotion regulation.

Despite evidence of abnormal functional connectivity across distributed brain networks in patients with MDD, it is unclear whether these differences reflect the state of current depression versus neurobiological traits that predispose individuals to be at risk for MDD. One approach to distinguishing between current state and predisposing traits is the study of unaffected individuals at heightened risk for MDD, such as unaffected children at familial risk for MDD by virtue of having a parent with MDD. Such familial history increases the risk of MDD in offspring by threefold to fivefold (30) and increases the risk of a broader spectrum of mood and anxiety disorders (31). Understanding whether rs-fMRI findings represent trait or state markers of MDD in the young can lead to the identification of informative neural biomarkers of risk for mood and anxiety disorders and help develop early intervention strategies to mitigate this risk. Resting-state fMRI also possesses significant translational strengths in its short duration of scanning and the lack of task performance demands that can complicate interpretation of activations.

In the present study, we examined rs-fMRI in unaffected children at familial risk for MDD and other mood and anxiety disorders by virtue of being offspring of parents with MDD (at-risk group) and compared them with age-matched children who were offspring of parents with no lifetime history of any mood disorder (control group). Two previous studies examining at-risk children and adolescents found decreased connectivity between the amygdala and frontal-parietal network in unaffected children of depressed mothers and in children with early-onset depression (29) and decreased connectivity within the frontal-parietal cognitive control network in unaffected adolescent girls with parental depression (32).

Based on previous functional connectivity results in patients with MDD, we focused on functional connectivity differences between at-risk and control children in the DMN, the cognitive control network, and the affective network, using a seed-based functional connectivity approach. We examined connectivity differences from the two midline anchor regions of the DMN (mPFC and PCC), which are associated with self-referential processing (33) and self-focused rumination in MDD (20,34), and from seed regions in left and right DLPFC and amygdala. We tested 1) whether unaffected at-risk children exhibit patterns of abnormal functional connectivity similar to those reported in patients with MDD, and 2) whether connectivity of DMN-sgACC is related to symptom scores in at-risk children. To further test whether resting-state connectivity can be a useful neural biomarker for risk for MDD, we built classification models based on resting-state data to discriminate at-risk versus control children.

METHODS AND MATERIALS

Participants

We initially recruited 38 offspring, 8 to 14 years of age, of parents with a lifetime history of MDD (at-risk group) and 30 age-matched offspring of parents with no lifetime mood disorder (control group). The study was approved by the Institutional Review Boards at Massachusetts General Hospital and at Massachusetts Institute of Technology. Parents provided written informed consent for their and their child's participation, and youths provided written assent. Exclusion criteria included the presence of acute psychosis or suicidality in a parent or a child, the presence at any point in the life span of bipolar disorder in the parent, autism in the child, or a lifetime history of a traumatic brain injury or neurological disorder in the child.

The final sample included in the analyses consisted of 27 at-risk and 16 control participants with no prior history of depression or current clinical-range symptom scores. Participants who did not complete the scan, had excessive head movement during the scan, or had a history of depression or clinical-range symptom scores were excluded. See Supplement for details.

Diagnostic Assessment

At enrollment for the present study, each child and both parents in each family were assessed for current and lifetime mood disorders (MDD, bipolar disorder, and dysthymia), using structured clinical interviews in which the mother was the informant. Interviews about parents used the depression, mania, dysthymia, and psychosis modules from the Structured Interview for DSM-IV (35) and those about the child used the depression, mania, dysthymia, and psychosis modules from the Schedule of Affective Disorders and Schizophrenia for School-Aged Children–Epidemiological Version for DSM-IV (36).

Other Assessments

Cognitive Function. To compare cognitive function between groups, we used the Kaufman Brief Intelligence Test-2, a 20-minute screen for verbal and nonverbal cognitive functioning (37).

Current Symptoms, Parent Report. To assess current behavioral and emotional symptoms in the children, we asked mothers to complete the Child Behavior Checklist (CBCL) (38) (see Supplement for details) about all children. The CBCL includes a total problems score, as well as scores reflecting internalizing (affective and anxiety) and externalizing symptoms (attentional problems and disruptive behavior). T-scores of 70 and above have been shown to discriminate clinical-range from nonclinical-range children (38).

Current Symptoms, Self-Report. To assess current depressive symptoms by self-report, we administered the Child Depression Inventory (CDI) (39) to all children. See Supplement for details of the CDI.

Participant Demographics

Children in the at-risk and control groups did not differ significantly in age, gender distribution, or IQ (ps > .3) (Table 1). The at-risk group had marginally higher CBCL total (p = .05), internalizing (p = .096), and anxiety (p = .08) scores but did not differ significantly in CBCL external problem scores (p = .34). None of the children had clinical-range CBCL scores (>70). CDI total scores did not differ significantly

Table 1. Participant Demographic and Clinical Information

	Control ($n = 16$)	At-risk ($n = 27$)	Statistical Evaluation
Age	11.3 ± 2.14	11.2 ± 1.67	$t_{41} = 0.17$, $p = .86$
Gender	8 F, 8 M	13 F, 14 M	$\chi^2 = 0.14$, $p = .9$
IQ (KBIT)	117 ± 10.5	120.6 ± 12.0	$t_{41} = 0.99$, $p = .33$
Mother Affected	0	18	
Father Affected	0	14	
Both Parents Affected	0	5	
CBCL Total	41.0 ± 11.8	48.8 ± 10.0	$t_{35} = 2.07$, $p = .046$
CBCL Internalizing	44.3 ± 8.50	50.1 ± 9.83	$t_{35} = 1.71$, $p = .096$
CBCL Externalizing	45.1 ± 10.5	47.8 ± 9.30	$t_{35} = 0.96$, $p = .34$
CBCL Anxiety	51.5 ± 2.78	55.2 ± 6.56	$t_{35} = 1.79$, $p = .08$
CDI	4.33 ± 5.54	6.57 ± 4.64	$t_{35} = 1.16$, $p = .26$

Values are mean ± SD where appropriate.

CBCL, Child Behavior Checklist; CDI, total score on the Child Depression Inventory; F, female; KBIT, Kaufman Brief Intelligence Test; M, male; p, between-group test p value; t(df), between-group t statistic and degrees of freedom.

between the two groups ($p = .26$). Additionally, by parent report, the children were largely prepubertal (with the exception of four at-risk and three control children).

Imaging Procedure

Data were acquired on a 3T TrioTim Siemens scanner (Siemens, Erlagen, Germany) using a 32-channel head coil. T1-weighted whole-brain anatomical images (magnetization prepared rapid acquisition gradient-echo sequence, 256 × 256 voxels, 1 × 1.3 mm in-plane resolution, 1.3-mm slice thickness) were acquired. After the anatomical scan, participants underwent a resting fMRI scan in which participants were instructed to keep their eyes open and the screen was blanked. Resting scan images were obtained in 67 2-mm-thick transverse slices, covering the entire brain (interleaved echo planar image sequence, T2*-weighted images; repetition time = 6 seconds, echo time = 30 ms, flip angle = 90, 2 × 2

× 2 mm voxels). The resting scan lasted 6.2 minutes (62 volumes). Online prospective acquisition correction was applied to the echo planar image sequence (40) (Supplement). Two dummy scans were included at the start of the sequence.

Functional Connectivity Analysis

Resting-state fMRI data were first preprocessed in SPM8 (Wellcome Trust Center for Neuroimaging, University College London, United Kingdom), using standard spatial preprocessing steps. Images were slice-time corrected, realigned to the first image of the resting scan, resampled such that they matched the first image of the resting scan voxel for voxel, normalized in Montreal Neurological Institute space, and smoothed with a 6-mm kernel (full width at half maximum). Functional connectivity analysis was performed using a seed-driven approach with in-house, custom software CONN (41,42). We performed seed-voxel correlations by estimating maps showing temporal correlations between the blood oxygen level–dependent signal from our a priori regions of interest (ROIs) and that at every brain voxel. We performed resting-state connectivity analysis from the DMN seeds (mPFC, PCC), cognitive control network seeds (bilateral DLPFC), and bilateral amygdala seeds (Figure 1). The DMN and DLPFC seeds were defined as 6-mm spheres around peak coordinates from Fair et al. (43). The amygdala seeds were defined from the WFU Pick Atlas (Wake Forest University School of Medicine, Winston-Salem, North Carolina) (44).

Physiological and other spurious sources of noise were estimated and regressed out using the anatomical CompCor method (aCompCor) (45). Global signal regression, a widely used preprocessing method, was not used because it artificially creates negative correlations that prevent the interpretation of anticorrelation (46) and can contribute to spurious group differences in positive correlations (47). Instead, aCompCor allows for interpretation of anticorrelations and yields higher specificity and sensitivity compared with global signal regression (41). See Supplement for details on the
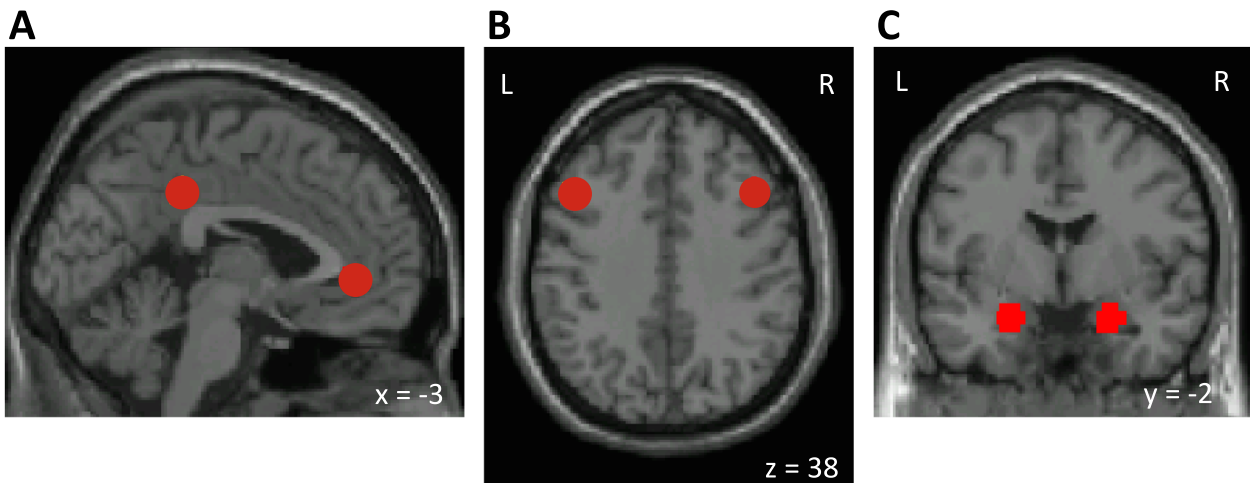

Figure 1. Seeds (regions of interest) used in the study. **(A)** Default mode network seeds (posterior cingulate cortex and medial prefrontal cortex); **(B)** left and right dorsolateral prefrontal cortex seeds; and **(C)** left and right amygdala seeds. Images are presented in neurological convention in all figures (left side of the brain is on the left side of the image). L, left hemisphere; R, right hemisphere.

aCompCor. A temporal band-pass filter of .008 Hz to .083 Hz was applied simultaneously to all regressors in the model. Residual head motion parameters (three rotation and three translation parameters plus another six parameters representing their first-order temporal derivatives) were regressed out. Artifact/outlier scans (average intensity deviated more than 3 standard deviations from the mean intensity in the session or composite head movement exceeded 1 mm from the previous image) were also regressed out. Head displacement across the resting scan did not differ significantly between the two groups for either frame-to-frame translations in x, y, z directions (at-risk group: mean = .19 mm ± .11; control group: mean = .16 mm ± .11; p = .33) or frame-to-frame rotations (at-risk group: mean = .0044 ± .002; control group: mean = .004 ± .003; p = .66). The number of outliers also did not differ significantly between the groups (range: 0 to 9; at-risk group: mean = 2.7 ± 2.2; control group: mean = 2.1 ± 3.1; p = .47). Outlier images were modeled as nuisance covariates. Each outlier image was represented by a single regressor in the general linear model, with a 1 for the outlier time point and 0 elsewhere.

Time series of all the voxels within each seed were averaged, and first-level correlation maps were produced by extracting the residual blood oxygen level–dependent time course from each seed and computing Pearson correlation coefficients between that time course and the time course of all other voxels. Correlation coefficients were converted to normally distributed Z scores using the Fisher transformation to allow for second-level general linear model analyses. DMN connectivity was calculated from the averages of the time series from mPFC and PCC seeds ([48],[49]), given their similar connectivity patterns. Functional connectivity of left and right DLPFC were analyzed separately, as were left and right amygdala, due to evidence of differential roles in emotion processing ([50]). First-level connectivity maps for each participant were entered into a between-group t test to determine connectivity differences for each seed between groups. Cluster-level threshold was set at p < .05 using false

discovery rate correction for multiple comparisons ([51]), with voxelwise t value threshold of 2.42 (df = 41; p < .01). Bonferroni correction was applied to the false discovery rate-corrected cluster-level p values to correct for multiple comparisons of the five a priori seeds tested (DMN, left and right DLPFC, and left and right amygdala). Regions that showed significant connectivity differences between groups were further examined for their connectivity values (significantly above or below zero) using one-sample t tests in each group. Based on prior evidence of DMN-sgACC hyperconnectivity in MDD and its implication in depressive rumination ([20]), we examined the within-group correlations between DMN-sgACC connectivity values and CBCL scores. Given the higher CBCL total scores in the at-risk group, we retested group differences by including CBCL total scores as a covariate.

Classification Models of At-Risk Children and Control Subject Discrimination

We trained two linear classification models using logistic regression, implemented in machine learning software Weka (University of Waikato, Hamilton, Waikato, New Zealand) ([52]), to categorize individual participants to the at-risk or control groups based on their rs-fMRI or behavioral data. To create robust prediction models that can be generalized to new cases, we performed leave-one-out cross-validation so that each individual was classified on the basis of data from the other individuals. Specifically, data from all participants except one were used as the training set to build a classification model, and the remaining participant was classified with the model and used as the validation case. This procedure was iterated for each participant and used to estimate specificity/sensitivity from the out-of-sample predictions. In the first model, we used anatomically defined ROIs that were independent from the regions that showed between-group connectivity differences. Connectivity values between the five a priori seeds and 116 clusters defined by the Automated
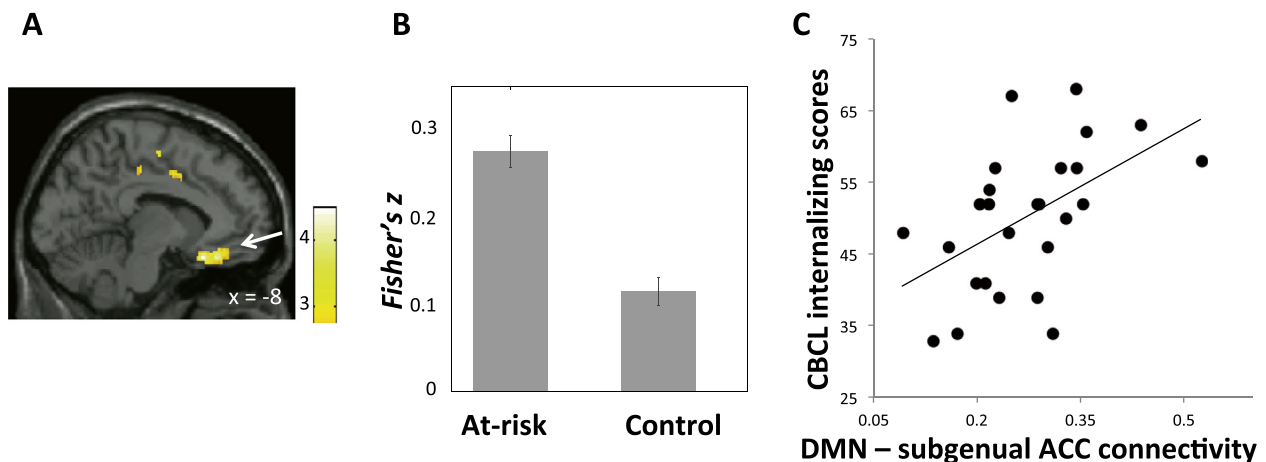

Figure 2. **(A)** Region in subgenual anterior cingulate cortex (ACC)/orbitofrontal cortex (OFC) (white arrow) that exhibited higher connectivity with the default mode network (DMN) in the at-risk than the control group. Color bar represents t values from between-group t test (at-risk > control). **(B)** Mean DMN-subgenual ACC/OFC connectivity (Fisher's z) in each group. Error bars represent standard errors of the means. **(C)** DMN-subgenual ACC/OFC connectivity plotted against Child Behavior Checklist (CBCL) internalizing scores within the at-risk group.

Table 2. Between-Group Connectivity Differences From Default Mode Network, Right Dorsolateral Prefrontal Cortex, Left Dorsolateral Prefrontal Cortex, and Right Amygdala

	BA	k (mm³)	x, y, z	t	p Value
Default Mode Network Connectivity					
At-risk > control					
L sgACC/OFC	25/11	2544	−8, 22, −20	4.44	< .001
R supramarginal gyrus	40	2152	64, −40, 26	4.47	< .001
R mid cingulum	24/31	2808	18, −34, 38	4.50	< .001
Control > at-risk					
None					
Right Dorsolateral Prefrontal Cortex Connectivity					
At-risk > control					
None					
Control > at-risk					
R DLPFC	46/9	2920	42, 28, 22	4.57	< .001
R inferior parietal lobule	40	1424	46, −50, 58	3.89	.01
Left Dorsolateral Prefrontal Cortex Connectivity					
At-risk > control					
Medial frontal gyrus	6/24	2072	0, −2, 48	3.66	.005
Control > at-risk					
R sgACC	25/11	2480	10, 18, −18	4.62	< .001
L inferior parietal lobule	40	2248	−50, −56, 54	4.93	.003
L lingual gyrus	18	2760	−14, −82, −14	5.77	< .001
R lingual gyrus	18	1976	32, −70, −14	4.24	< .001
R superior frontal gyrus	8/6	8616	14, 34, 60	5.25	< .001
R inferior temporal gyrus	21	8392	60, −14, −20	6.88	< .001
L inferior temporal gyrus	21	3120	−60, −14, −20	5.00	< .001
Right Amygdala Connectivity					
At-risk > control					
R inferior frontal gyrus	47	2608	44, 40, 4	4.41	< .001
R SMG/STG	40/22	1456	42, −40, 16	3.94	< .001
Control > at-risk					
None					

All reported clusters survived Bonferroni correction of p < .05 for the number of seeds tested (five).

Peak coordinates (x, y, z) based on Montreal Neurologic Institute brain.

BA, Brodmann area; DLPFC, dorsolateral prefrontal cortex; k, cluster size in mm³; L, left; OFC, orbitofrontal cortex; p Value, false discovery rate–corrected cluster-level p value; R, right; sgACC, subgenual anterior cingulate cortex; SMG, supramarginal gyrus; STG, superior temporal gyrus; t, peak t value from the cluster (degrees of freedom = 41).

Anatomical Labeling atlas (Université de Caen, Université de Paris 5, France) (53) were estimated and used in the prediction model. We constructed a second model based on CBCL scores (total, internalizing, externalizing, anxiety) to compare with classification accuracies from the model based on rs-fMRI data in anatomically defined ROIs.

RESULTS

Increased Connectivity Between DMN and sgACC/Orbitofrontal Cortex in At-Risk Children

Compared with the control group, the at-risk group exhibited increased positive DMN connectivity with a cluster in the sgACC extending into medial orbitofrontal cortex (OFC) bilaterally (Figure 2A, B; Table 2). Among the at-risk children, connectivity between the DMN and sgACC/OFC correlated significantly and positively with CBCL internalizing scores (at-risk: r = .53, p = .003; Figure 2C) and CBCL total scores

(at-risk: r = .39, p = .04); there was no such correlation among the control children. Connectivity strengths within the DMN did not differ significantly between groups.

Decreased Anticorrelation Between DMN and Inferior Parietal Lobule in At-Risk Children

Compared with the control group, the at-risk group exhibited higher positive connectivity between the DMN and the right inferior parietal lobule (IPL) (Figure 3; Table 2). Instead of the anticorrelation exhibited in the control group (t_{15} = −5.99, p = .004), the at-risk group exhibited a positive correlation between the DMN and the right IPL (t_{29} = 2.25, p = .03).

Decreased Connectivity Within Cognitive Control Network in At-Risk Children

Compared with the control group, the at-risk group exhibited decreased positive connectivity between the right DLPFC seed and the right frontal-parietal control network regions,
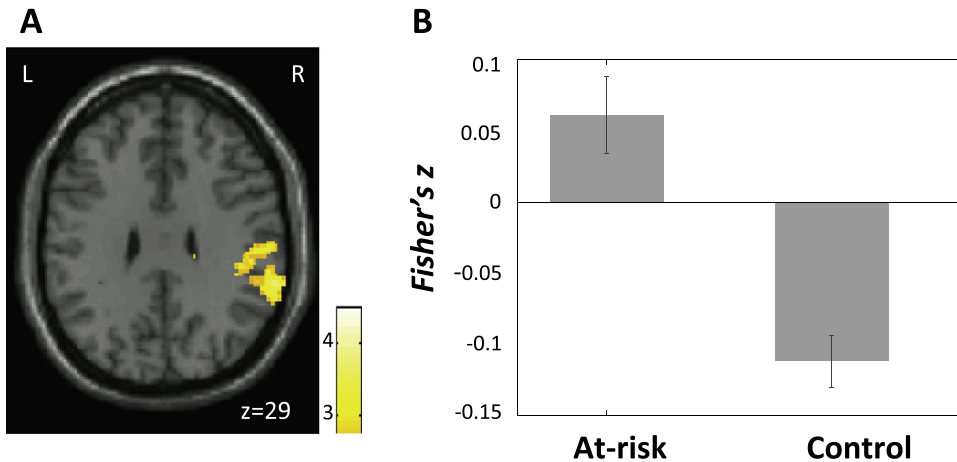
Figure 3. (A) Region in the right inferior parietal lobule that exhibited higher connectivity with the default mode network in the at-risk than the control group. Color bar represents *t* values from between-group *t* test (at-risk > control). (B) Mean connectivity between default mode network and the inferior parietal lobule cluster shown in (A) in each group. Error bars represent standard errors of the means. L, left hemisphere; R, right hemisphere.

including the right IPL and the right DLPFC (Brodmann area 46) (Figure 4; Table 2) and decreased connectivity between left DLPFC seed and the left IPL (Table 2).

Decreased Connectivity Between Left DLPFC and sgACC in At-Risk Children

Compared to the control group, the at-risk group exhibited decreased connectivity between the left DLPFC seed and sgACC (bilateral), right lingual gyrus, right superior frontal gyrus, and bilateral inferior temple gyri and increased connectivity between left DLPFC and supplementary motor cortex (Table 2). Left DLPFC and sgACC were anticorrelated in at-risk children only ($t_{29} = -3.36$, $p = .002$; Figure 5).

Increased Connectivity Between Amygdala and Inferior Frontal Gyrus in At-Risk Children

Compared with the control group, the at-risk group exhibited increased connectivity between the right amygdala and both the right inferior frontal gyrus (IFG) and the right supramarginal

gyrus (Figure 6; Table 2). Instead of the negative correlations exhibited in the control group, the at-risk group exhibited positive correlations between right amygdala and right IFG (control group: $t_{15} = -3.54$, $p = .003$; at-risk group: $t_{29} = 4.67$, $p < .001$) and between right amygdala and right supramarginal gyrus (control group: $t_{15} = -2.53$, $p = .02$; at-risk group: $t_{29} = 4.53$, $p < .001$). Connectivity from the left amygdala did not differ between the two groups.

Group Differences After Controlling for Symptom Scores

After controlling for CBCL total scores, differences between the at-risk and control groups remained largely similar to the above reported results (Supplemental Table S1).

Classification of At-Risk Children and Control Subjects

The classification model based on connectivity data in ROIs defined from the Automated Anatomical Labeling atlas (Université de Caen, Université de Paris 5) yielded 79% accuracy,
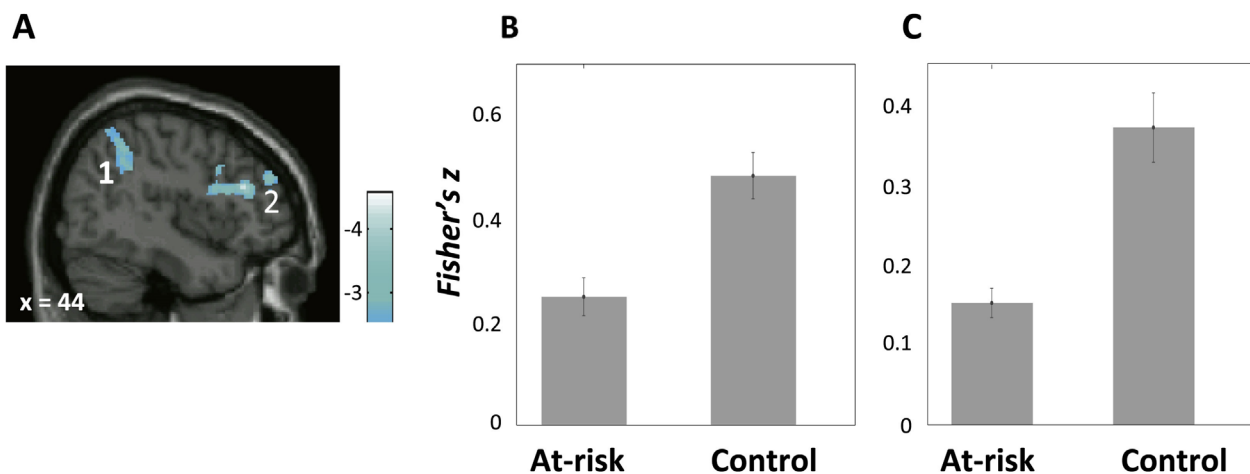

Figure 4. (A) Regions that exhibited lower connectivity with right dorsolateral prefrontal cortex (DLPFC) seed in the at-risk than the control group; (1) right inferior parietal lobule; (2) right DLPFC. Color bar represents *t* values from between-group *t* test (control > at-risk). (B) Mean connectivity (Fisher's z) between the right DLPFC seed and the right inferior parietal lobule cluster (1) in each group. (C) Mean connectivity (Fisher's z) between the right DLPFC seed and a cluster in the right DLPFC (2) in each group. Error bars represent standard errors of the means.
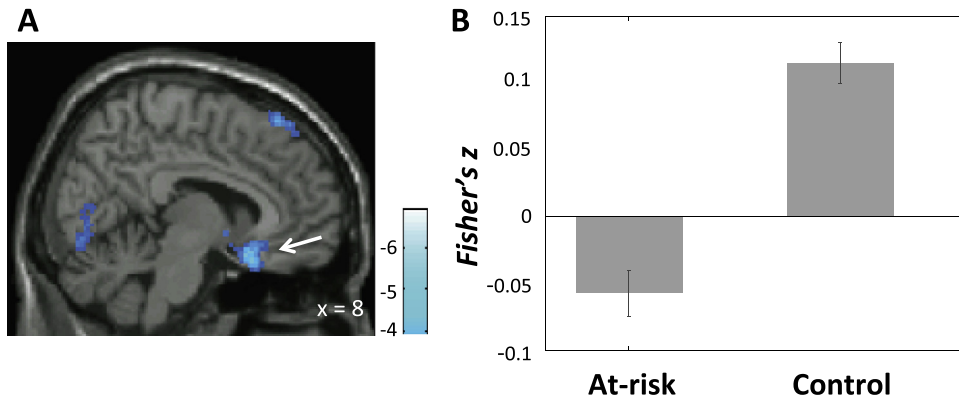
Figure 5. **(A)** Region in the subgenual anterior cingulate cortex (white arrow) that exhibited lower connectivity with left dorsolateral prefrontal cortex seed in the at-risk than the control group. Color bar represents *t* values from between-group *t* test (control > at-risk). **(B)** Mean connectivity (Fisher's z) between the left dorsolateral prefrontal cortex seed and the subgenual anterior cingulate cortex cluster shown in **(A)** in each group. Error bars represent standard errors of the means.

81% sensitivity, and 78% specificity. The model based on CBCL scores yielded only 64% accuracy with 80% sensitivity and 27% specificity.

DISCUSSION

We found differential intrinsic functional connectivity patterns in unaffected children with familial risk for MDD compared with children without such familial risk in the DMN, the cognitive control network, and the amygdala. At-risk children showed hyperconnectivity between the DMN and the sgACC/OFC. Furthermore, although none of the at-risk children were clinically depressed, DMN-sgACC/OFC connectivity was positively correlated with individual CBCL scores among those children. At-risk children also showed hypoconnectivity within the cognitive control network, lacked the typical anticorrelation between the DMN and the right parietal region, and exhibited lower connectivity between left DLPFC and sgACC. In addition, at-risk children showed hyperconnectivity between amygdala and the right IFG. Finally, classification between at-risk children and control subjects based on resting-state connectivity yielded high sensitivity and specificity. These findings appear to identify trait neurobiological underpinnings of risk for major depression in the absence of the state of depression.

Increased connectivity between DMN and sgACC in at-risk children and the positive correlation between DMN-sgACC connectivity and current symptom scores are consistent with findings reported in adult (16,17) and pediatric (19) patients with MDD. The fact that these findings were observed in unaffected children at familial risk for MDD suggests that hyperconnectivity with sgACC is not a consequence or manifestation of MDD but instead may be a biomarker of predisposed risk for MDD. The at-risk children also exhibited an atypical anticorrelation between sgACC and left DLPFC. In line with our finding, stimulation of the sgACC resulted in attenuation of hyperactivation in sgACC and increased activation in previously underactive DLPFC in adults with MDD (54). The left DLPFC region that showed maximum anticorrelation with the sgACC has been identified as a target for transcranial magnetic stimulation treatment of MDD (55). A prospective study would be needed to determine if atypical sgACC connectivity at this age predicts later development of MDD.

The lack of typical anticorrelation between the DMN and supramarginal gyrus/inferior parietal lobule, an important attention control region (56,57), in at-risk children is consistent with cognitive control deficits in depressed adult patients (58,59) and reduced DMN deactivation during an emotional identification task in depressed adolescents (3). Greater
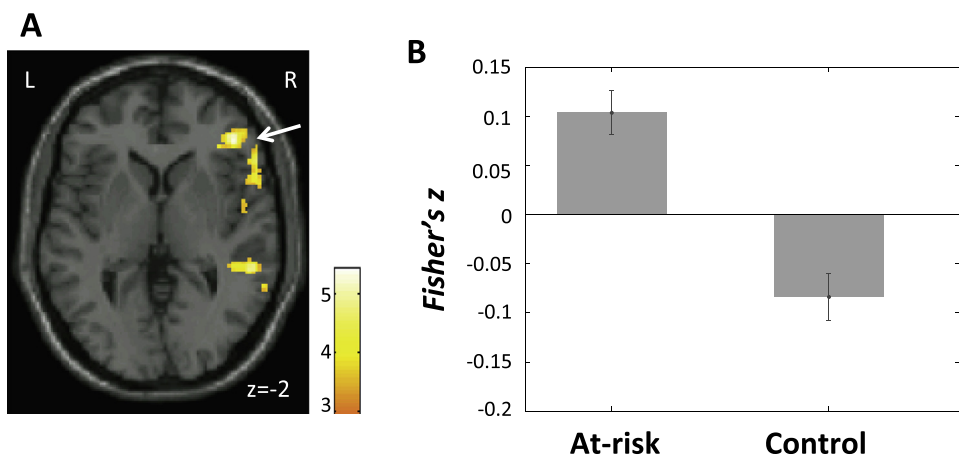

Figure 6. **(A)** Region in the right inferior frontal gyrus (white arrow) that exhibited higher connectivity with right amygdala seed in the at-risk than the control group. Color bar represents *t* values from between-group *t* test (at-risk > control). **(B)** Mean connectivity (Fisher's z) between the right amygdala seed and the right inferior frontal gyrus cluster shown in **(A)** in each group. Error bars represent standard errors of the means. L, left hemisphere; R, right hemisphere.

anticorrelation between DMN and cognitive control networks in healthy adults has been linked to better performance in cognitive control and working memory tasks (60,61) and may reflect an individual's capacity to switch between internally and externally focused attention (62). This dynamic interplay between DMN and cognitive control networks in MDD was examined in a task-based connectivity study. During an external attention condition, adults with MDD exhibited increased DMN connectivity and decreased cognitive control network connectivity (25). The present study suggests that an imbalance between DMN and cognitive control networks is a developmental risk factor for MDD.

With regard to decreased connectivity within the cognitive control regions in at-risk children, a previous study of adolescents with familial risk for depression also reported reduced connectivity between cognitive control regions (32). In that study, lower connectivity in the control network was associated with more severe parental depression symptoms. These results in at-risk children and adolescents are consistent with findings from depressed adults of reduced connectivity in attention control regions including the DLPFC (23). Studies consistently show that the DLPFC is underactivated in depressed adults (63), which might contribute to their difficulty in cognitive control and emotion regulation (64). It is possible that children at risk for depression have an underconnected control network that is also a developmental risk factor for MDD.

There was increased connectivity between the right amygdala and the right IFG and supramarginal gyrus in at-risk children. The right IFG is a key region in emotion regulation (65). The top-down IFG-amygdala circuitry is disrupted during emotion regulation in adults with mood disorders (66,67). A study of children with MDD and children of mothers with MDD also reported reduced negative correlation between the amygdala and lateral parietal regions including the supramarginal gyrus (29). The atypically high level of connectivity between amygdala and emotion regulation and cognitive control regions might reflect emotion dysregulation in MDD.

To test whether intrinsic functional organization of the brain, as measured by rs-fMRI, can be a potential biomarker for risk for depression in children, we performed a classification analysis to discriminate children in the at-risk group and control group based on their resting-state functional connectivity data. This classification based on functional connectivity yielded high accuracy, sensitivity, and specificity in discriminating between children at risk for MDD and control subjects compared with classification based on CBCL scores. Importantly, the rs-fMRI classification was based on analyses that, at the level of each individual child, were independent of the group differences in functional connectivity. Such generalizable and individually robust classification is important if brain measures are to be used for early identification (68). Future prospective and longitudinal studies can determine whether such biomarkers predict which high-risk children progress to MDD and whether early intervention reduces the likelihood of developing MDD. Also, perhaps such biomarkers may be helpful in identifying children at risk for developing depression independent of parental histories of depression.

Our findings need to be viewed in light of some methodological limitations. First, we did not exclude children born prematurely, and premature births can lead to neurological complications. However, we did exclude children with known developmental delays such as autism and intellectual disability. Second, because parental MDD confers a spectrum of risk to offspring (31,69), the at-risk children were also at risk for anxiety and other disorders. Parents with MDD also have higher rates of comorbid anxiety than the general population. Thus, we cannot rule out that the brain differences we found were due to the risk for anxiety and other disorders in these children. Third, although our sample size of at-risk children ($n = 27$) was moderate, the control group was small ($n = 16$). Lastly, our resting-state scans were acquired with a repetition time (TR) of 6 seconds, which is longer than most resting-state fMRI studies so that we could acquire high-resolution whole-brain data (2-mm isotropic voxels) without the use of parallel imaging. A previous study found there was no significant difference in correlation strengths within and between resting-state functional networks when comparing resting scans of TR = 2.5 seconds and TR = 5 seconds and that correlation strengths stabilized with acquisition time of 5 minutes (TR = 5) (70). In the current and previous studies using the same acquisition parameters (TR = 6 seconds) (71), we observed the typical resting-state network patterns observed in other studies. Nonetheless, an additional issue of the long TR is that cognitive and emotional processes internally initiated at the beginning and the end of each scan can be different. We cannot rule out the possibility that the group difference observed here might be, in part, due to systematic differences in chronometry between the two groups.

The present study consisted of a sample of preadolescent children who were at familial risk for depression but not currently affected with depression, and therefore, functional connectivity differences cannot reflect an expression of depression as could be the case in patients with ongoing MDD. Rather, the differences in intrinsic functional brain architecture likely reflect neural traits that predispose children toward MDD or related disorders. Importantly, we demonstrated that discrimination between at-risk and control children occurred with high sensitivity and specificity based on resting-state functional connectivity. Future studies that track the development of children at familial risk for MDD and determine which children develop MDD or other mood and anxiety disorders are needed to build predictive models based on findings from the present study so as to identify high-risk individuals for early intervention.

ARTICLE INFORMATION

REFERENCES

1. Grimm S, Boesiger P, Beck J, Schuepbach D, Bermpohl F, Walter M, et al. (2009): Altered negative BOLD responses in the default-mode network during emotion processing in depressed subjects. Neuropsychopharmacology 34; 932–843.
2. Sheline YI, Barch DM, Price JL, Rundle MM, Vaishnavi SN, Snyder AZ, et al. (2009): The default mode network and self-referential processes in depression. Proc Natl Acad Sci U S A 106:1942–1947.
3. Ho TC, Connolly CG, Henje Blom E, LeWinn KZ, Strigo IA, Paulus MP, et al. (2015): Emotion-dependent functional connectivity of the default mode network in adolescent depression. Biol Psychiatry 78:635–646.
4. Fales CL, Barch DM, Rundle MM, Mintun MA, Snyder AZ, Cohen JD, et al. (2008): Altered emotional interference processing in affective and cognitive-control brain circuitry in major depression. Biol Psychiatry 63:377–384.
5. Mitterschiffthaler MT, Williams SCR, Walsh ND, Cleare AJ, Donaldson C, Scott J, Fu CHY (2008): Neural basis of the emotional Stroop interference effect in major depression. Psychol Med 38:247–256.
6. Sheline YI, Price JL, Yan Z, Mintun MA (2010): Resting-state functional MRI in depression unmasks increased connectivity between networks via the dorsal nexus. Proc Natl Acad Sci U S A 107:11020–11025.
7. Zeng LL, Shen H, Liu L, Wang L, Li B, Fang P, et al. (2012): Identifying major depression using whole-brain functional connectivity: A multivariate pattern analysis. Brain 135:1498–1507.
8. Mayberg HS (1997): Limbic-cortical dysregulation: A proposed model of depression. J Neuropsychiatry Clin Neurosci 9:471–481.
9. Drevets WC, Price JL, Simpson JR, Todd RD, Reich T, Vannier M, Raichle ME (1997): Subgenual prefrontal cortex abnormalities in mood disorders. Nature 386:824–827.
10. Ongür D, Drevets WC, Price JL (1998): Glial reduction in the subgenual prefrontal cortex in mood disorders. Proc Natl Acad Sci U S A 95:13290–13295.
11. Gotlib IH, Sivers H, Gabrieli JDE, Whitfield-Gabrieli S, Goldin P, Minor KL, Canli T (2005): Subgenual anterior cingulate activation to valenced emotional stimuli in major depression. Neuroreport 16:1731–1734.
12. Sheline YI, Barch DM, Donnelly JM, Ollinger JM, Snyder AZ, Mintun MA (2001): Increased amygdala response to masked emotional faces in depressed subjects resolves with antidepressant treatment: An fMRI study. Biol Psychiatry 50:651–658.
13. Suslow T, Konrad C, Kugel H, Rumstadt D, Zwitserlood P, Schöning S, et al. (2010): Automatic mood-congruent amygdala responses to masked facial expressions in major depression. Biol Psychiatry 67:155–160.
14. Disner SG, Beevers CG, Haigh EAP, Beck AT (2011): Neural mechanisms of the cognitive model of depression. Nat Rev Neurosci 12:467–477.
15. Kaiser RH, Andrews-Hanna JR, Wager TD, Pizzagalli DA (2015): Large-scale network dysfunction in major depressive disorder. JAMA Psychiatry 02478:1–10.
16. Greicius MD, Flores BH, Menon V, Glover GH, Solvason HB, Kenna H, et al. (2007): Resting-state functional connectivity in major depression: Abnormally increased contributions from subgenual cingulate cortex and thalamus. Biol Psychiatry 62:429–437.
17. Zhou Y, Yu C, Zheng H, Liu Y, Song M, Qin W, et al. (2010): Increased neural resources recruitment in the intrinsic organization in major depression. J Affect Disord 121:220–230.
18. Connolly CG, Wu J, Ho TC, Hoeft F, Wolkowitz O, Eisendrath S, et al. (2013): Resting-state functional connectivity of subgenual anterior cingulate cortex in depressed adolescents. Biol Psychiatry 74:898–907.
19. Gaffrey MS, Luby JL, Repovš G, Belden AC, Botteron KN, Luking KR, Barch DM (2010): Subgenual cingulate connectivity in children with a history of preschool-depression. Neuroreport 21:1182–1188.
20. Hamilton JP, Farmer M, Fogelman P, Gotlib IH (2015): Depressive rumination, the default-mode network, and the dark matter of clinical neuroscience. Biol Psychiatry 78:224–230.
21. Veer IM, Beckmann CF, van Tol M-J, Ferrarini L, Milles J, Veltman DJ, et al. (2010): Whole brain resting-state analysis reveals decreased functional connectivity in major depression. Front Syst Neurosci 4:41.
22. Alexopoulos GS, Hoptman MJ, Kanellopoulos D, Murphy CF, Lim KO, Gunning FM (2012): Functional connectivity in the cognitive control network and the default mode network in late-life depression. J Affect Disord 139:56–65.
23. Ye T, Peng J, Nie B, Gao J, Liu J, Li Y, et al. (2012): Altered functional connectivity of the dorsolateral prefrontal cortex in first-episode patients with major depressive disorder. Eur J Radiol 81:4035–4040.
24. Marchetti I, Koster EHW, Sonuga-Barke EJ, De Raedt R (2012): The default mode network and recurrent depression: A neurobiological model of cognitive risk factors. Neuropsychol Rev 22:229–251.
25. Belleau EL, Taubitz LE, Larson CL (2015): Imbalance of default mode and regulatory networks during externally focused processing in depression. Soc Cogn Affect Neurosci 10:744–751.
26. Hamilton JP, Chen MC, Gotlib IH (2013): Neural systems approaches to understanding major depressive disorder: An intrinsic functional organization perspective. Neurobiol Dis 52:4–11.
27. Anand A, Li Y, Wang Y, Wu J, Gao S, Bukhari L, et al. (2005): Activity and connectivity of brain mood regulating circuit in depression: A functional magnetic resonance study. Biol Psychiatry 57:1079–1088.
28. Chen C-H, Suckling J, Ooi C, Fu CHY, Williams SCR, Walsh ND, et al. (2008): Functional coupling of the amygdala in depressed patients treated with antidepressant medication. Neuropsychopharmacology 33:1909–1918.
29. Luking KR, Repovs G, Belden AC, Gaffrey MS, Botteron KN, Luby JL, Barch DM (2011): Functional connectivity of the amygdala in early-childhood-onset depression. J Am Acad Child Adolesc Psychiatry 50 (1027–1041):e3.
30. Williamson DE, Birmaher B, Axelson DA, Ryan ND, Dahl RE (2004): First episode of depression in children at low and high familial risk for depression. J Am Acad Child Adolesc Psychiatry 43:291–297.
31. Lieb R, Isensee B, Höfler M, Pfister H, Wittchen H-U (2002): Parental major depression and the risk of depression and other mental

disorders in offspring: A prospective-longitudinal community study. Arch Gen Psychiatry 59:365–374.

32. Clasen PC, Beevers CG, Mumford JA, Schnyer DM (2014): Cognitive control network connectivity in adolescent women with and without a parental history of depression. Dev Cogn Neurosci 7:13–22.

33. Whitfield-Gabrieli S, Moran JM, Nieto-Castañón A, Triantafyllou C, Saxe R, Gabrieli JDE (2011): Associations and dissociations between default and self-reference networks in the human brain. Neuroimage 55:225–232.

34. Nejad AB, Fossati P, Lemogne C (2013): Self-referential processing, rumination, and cortical midline structures in major depression. Front Hum Neurosci 7:666.

35. First MB, Spitzer RL, Gibbon M, Williams JBW (1995): Structured Clinical Interview for DSM-IV Axis I Disorders (Clinician Version). New York: New York State Psychiatric Institute Biometrics Department.

36. Orvaschel H (1994): 5th ed.In: Schedule for Affective Disorder and Schizophrenia for School-Age children–Epidemiologic Version, 5th ed. Fort Lauderdale, FL: Nova Southeastern University, Center for Psychological Studies.

37. Kaufman AS, Kaufman NL (2004): Kaufman Brief Intelligence Test, Second Edition (KBIT-2). Bloomington, MN: Pearson, Inc.

38. Achenbach TM, Rescorla LA (2001): In: Manual for ASEBA School-Age Forms & Profile. Burlington, VT: University of Vermont, Research Center for Children, Youth, & Families.

39. Kovacs M (1985): The Children's Depression, Inventory (CDI). Psychopharmacol Bull 21:995–998.

40. Thesen S, Heid O, Mueller E, Schad LR (2000): Prospective acquisition correction for head motion with image-based tracking for real-time fMRI. Magn Reson Med 44:457–465.

41. Chai XJ, Castañán AN, Öngür D, Whitfield-Gabrieli S (2012): Anti-correlations in resting state networks without global signal regression. Neuroimage 59:1420–1428.

42. Whitfield-Gabrieli S, Nieto-Castanon A (2012): Conn: A functional connectivity toolbox for correlated and anticorrelated brain networks. Brain Connect 2:125–141.

43. Fair DA, Cohen AL, Power JD, Dosenbach NUF, Church JA, Miezin FM, et al. (2009): Functional brain networks develop from a "local to distributed" organization. PLoS Comput Biol 5:14–23.

44. Maldjian JA, Laurienti PJ, Kraft RA, Burdette JH (2003): An automated method for neuroanatomic and cytoarchitectonic atlas-based interrogation of fMRI data sets. Neuroimage 19:1233–1239.

45. Behzadi Y, Restom K, Liau J, Liu TT (2007): A component based noise correction method (CompCor) for BOLD and perfusion based fMRI. Neuroimage 37:90–101.

46. Murphy K, Birn RM, Handwerker DA, Jones TB, Bandettini PA (2009): The impact of global signal regression on resting state correlations: Are anti-correlated networks introduced? Neuroimage 44:893–905.

47. Saad ZS, Gotts SJ, Murphy K, Chen G, Jo HJ, Martin A, Cox RW (2012): Trouble at rest: How correlation patterns and group differences become distorted after global signal regression. Brain Connect 2:25–32.

48. Whitfield-Gabrieli S, Thermenos HW, Milanovic S, Tsuang MT, Faraone SV, McCarley RW, et al. (2009): Hyperactivity and hyperconnectivity of the default network in schizophrenia and in first-degree relatives of persons with schizophrenia. Proc Natl Acad Sci U S A 106:1279–1284.

49. Fox MD, Snyder AZ, Vincent JL, Corbetta M, Van Essen DC, Raichle ME (2005): The human brain is intrinsically organized into dynamic, anticorrelated functional networks. Proc Natl Acad Sci U S A 102:9673–9678.

50. Dyck M, Loughead J, Kellermann T, Boers F, Gur RC, Mathiak K (2011): Cognitive versus automatic mechanisms of mood induction differentially activate left and right amygdala. Neuroimage 54:2503–2513.

51. Genovese CR, Lazar NA, Nichols T (2002): Thresholding of statistical maps in functional neuroimaging using the false discovery rate. Neuroimage 15:870–878.

52. Hall M, National H, Frank E, Holmes G, Pfahringer B, Reutemann P, Witten IH (2009): The WEKA data mining software: An update. SIGKDD Explor 11:10–18.

53. Tzourio-Mazoyer N, Landeau B, Papathanassiou D, Crivello F, Etard O, Delcroix N, et al. (2002): Automated anatomical labeling of activations in SPM using a macroscopic anatomical parcellation of the MNI MRI single-subject brain. Neuroimage 15:273–289.

54. Mayberg HS, Lozano AM, Voon V, McNeely HE, Seminowicz D, Hamani C, et al. (2005): Deep brain stimulation for treatment-resistant depression. Neuron 45:651–660.

55. Fox MD, Liu H, Pascual-Leone A (2013): Identification of reproducible individualized targets for treatment of depression with TMS based on intrinsic connectivity. Neuroimage 66:151–160.

56. Corbetta M, Kincade MJ, Lewis C, Snyder AZ, Sapir A (2005): Neural basis and recovery of spatial attention deficits in spatial neglect. Nat Neurosci 8:1603–1610.

57. Ptak R (2012): The frontoparietal attention network of the human brain: Action, saliency, and a priority map of the environment. Neuroscientist 18:502–515.

58. Hartlage S, Alloy LB, Vázquez C, Dykman B (1993): Automatic and effortful processing in depression. Psychol Bull 113:247–278.

59. Harvey PO, Le Bastard G, Pochon JB, Levy R, Allilaire JF, Dubois B, Fossati P (2004): Executive functions and updating of the contents of working memory in unipolar depression. J Psychiatr Res 38:567–576.

60. Keller JB, Hedden T, Thompson TW, Anteraper SA, Gabrieli JDE, Whitfield-Gabrieli S (2015): Resting-state anticorrelations between medial and lateral prefrontal cortex: Association with working memory, aging, and individual differences. Cortex 64:271–280.

61. Hampson M, Driesen N, Roth JK, Gore JC, Constable RT (2010): Functional connectivity between task-positive and task-negative brain areas and its relation to working memory performance. Magn Reson Imaging 28:1051–1057.

62. Whitfield-Gabrieli S, Ford JM (2012): Default mode network activity and connectivity in psychopathology. Annu Rev Clin Psychol 8:49–76.

63. Hooley JM, Gruber SA, Scott LA, Hiller JB, Yurgelun-Todd DA (2005): Activation in dorsolateral prefrontal cortex in response to maternal criticism and praise in recovered depressed and healthy control participants. Biol Psychiatry 57:809–812.

64. Gotlib IH, Hamilton JP (2008): Neuroimaging and depression: Current status and unresolved issues. Curr Dir Psychol Sci 17:159–163.

65. Wager TD, Davidson ML, Hughes BL, Lindquist MA, Ochsner KN (2008): Prefrontal-subcortical pathways mediating successful emotion regulation. Neuron 59:1037–1050.

66. Johnstone T, van Reekum CM, Urry HL, Kalin NH, Davidson RJ (2007): Failure to regulate: Counterproductive recruitment of top-down prefrontal-subcortical circuitry in major depression. J Neurosci 27:8877–8884.

67. Townsend JD, Torrisi SJ, Lieberman MD, Sugar CA, Bookheimer SY, Altshuler LL (2013): Frontal-amygdala connectivity alterations during emotion downregulation in bipolar I disorder. Biol Psychiatry 73:127–135.

68. Gabrieli JDE, Ghosh SS, Whitfield-Gabrieli S (2015): Prediction as a humanitarian and pragmatic contribution from human cognitive neuroscience. Neuron 85:11–26.

69. Hirshfeld-Becker DR, Micco JA, Henin A, Petty C, Faraone SV, Mazursky H, et al. (2012): Psychopathology in adolescent offspring of parents with panic disorder, major depression, or both: A 10-year follow-up. Am J Psychiatry 169:1175–1184.

70. Van Dijk KRA, Hedden T, Venkataraman A, Evans KC, Lazar SW, Buckner RL (2010): Intrinsic functional connectivity as a tool for human connectomics: Theory, properties, and optimization. J Neurophysiol 103:297–321.

71. Redcay E, Moran JM, Mavros PL, Tager-Flusberg H, Gabrieli JDE, Whitfield-Gabrieli S (2013): Intrinsic functional network organization in high-functioning adolescents with autism spectrum disorder. Front Hum Neurosci 7:573.